International Journal of Nanomedicine

Dovepress
Taylor & Francis Group

Open Access Full Text Article

ORIGINAL RESEARCH

Carbon-Encapsulated Iron Nanoparticles Seeking Integrins in Murine Glioma

Agnieszka Stawarska[1,*], Magdalena Bamburowicz-Klimkowska[1,*], Michał Bystrzejewski[2], Artur Kasprzak[3], Ireneusz P Grudzinski[1]

[1]Department of Toxicology and Food Science, Faculty of Pharmacy, Medical University of Warsaw, Warsaw, Poland; [2]Department of Physical Chemistry, Faculty of Chemistry, Warsaw University, Warsaw, Poland; [3]Department of Organic Chemistry, Faculty of Chemistry, Warsaw University of Technology, Warsaw, Poland

*These authors contributed equally to this work

Correspondence: Agnieszka Stawarska, Email agnieszka.stawarska@wum.edu.pl

Purpose: Targeting integrin receptors for MRI represents a novel method in diagnosing glioblastoma. In the present study carbon-encapsulated iron nanoparticles to explore murine glioma tracking based upon specific direct targeting with monoclonal antibodies against the beta-3 subunit (CD61) of the integrin αVβ3 receptor are described.

Methods: The carbon arc discharge method was used to synthesize nanoparticles and amidation-type reaction were applied to attach monoclonal antibody (anti-CD61) with acidic group functionalized nanoparticles to lead two types of bioconjugates (Fe@C-CONH-anti-CD61 and Fe@C-$(CH_2)_2$-CONH-anti-CD61). The as-synthesized bioconjugates were tested on murine glioma cells (GL261) using MTT, LDH and calcein AM/propidium iodide assays. Relaxometry measurements were performed with a 1.5 T (63 MHz) MRI scanner using both GL261 cells and C57BL/6 mice bearing GL261 tumors.

Results: The results showed that Fe@C-CONH-anti-CD61 and Fe@C-$(CH_2)_2$-CONH-anti-CD61 nanoparticles have higher binding affinity towards GL261 cells compared to pristine nanoparticles without antibodies. Studies evidenced that the antibody-decorated nanoparticles did not produce any severe cytotoxic effects on murine glioma cells. Preclinical MRI studies demonstrated that the Fe@C-$(CH_2)_2$-CONH-anti-CD61 nanoparticle-based construct specifically targeted murine glioma in animals.

Conclusion: The carbon-encapsulated iron nanoparticles functionalized with monoclonal antibodies recognizing the beta-3 subunit of the integrin αVβ3 receptor can be considered as a potential contrast agent for MRI-based tracking glioblastoma.

Keywords: carbon-encapsulated iron nanoparticles, monoclonal antibodies, glioblastoma, integrins, cytotoxicity, magnetic resonance imaging

Introduction

Glioblastoma is the most malignant primary brain tumor in adults with an extremely poor prognosis, as the median 5-year overall survival rate is less than 20%.[1] These tumors account for more than 80% of all brain malignancies and constitute approximately 30% of all brain tumors.[2,3] The starting point in primary diagnosis, which involves determining the location, size, and type of the tumor, consists of conventional diagnostic methods such as computed tomography (CT), positron emission tomography (PET) and magnetic resonance imaging (MRI).[4,5] These methods play a fundamental role, serving as the basis for further advanced diagnostics and disease management.[6,7]

MRI plays a key role in diagnosing, characterizing, monitoring, and evaluating the treatment of gliomas, providing high-resolution structural details and MRI has the highest degree of confidence in glioma diagnosis.[8] MRI being the imaging modality of choice owing to a higher sensitivity than among others CT in determining the size, number, and distribution of central nervous system lesions.[9] However, one of the significant limitations of conventional MRI is its poor biological specificity, particularly in distinguishing active tumor areas.[3,10] Advances in the genetic biology of gliomas and the recent introduction of experimental manipulation models may contribute to the development of effective

Received: 5 February 2025
Accepted: 9 April 2025
Published: 28 April 2025

Graphical Abstract

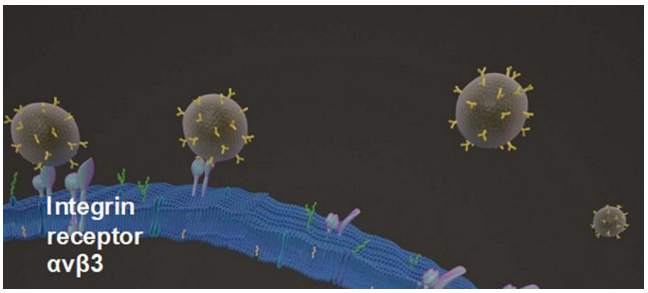

diagnostic methods and targeted therapies.[11] Conventional diagnostic and therapeutic agents often show improper biodistribution due to the challenging blood-brain barrier.[12] Furthermore, they are nonspecific and may accumulate in healthy organs, leading to high toxicity. Commonly used clinical contrast agents, such as gadolinium-based agents or radiopharmaceuticals, are excreted by the kidneys within a short period. However, their accumulation in non-target organs, especially with repeated or prolonged use, can still lead to toxicity. While the accumulation of these agents in healthy tissues is a primary cause of toxicity, their chemical properties and interactions with cellular structures also contribute to adverse effects. For instance, certain gadolinium-based agents have been associated with nephrogenic systemic fibrosis (NSF) in patients with impaired renal function, underscoring that toxicity can arise not only from accumulation but also from other factors.[13] One potential solution to this issue is the nanotheranostic approach. For instance, nanoparticle-enhanced imaging of the central nervous system at the subcellular level allows for more precise localization of intracranial tumor areas.[14,15]

Recent studies have highlighted the potential of magnetic nanoparticles (MNPs) as nanocarriers for targeted drug delivery and imaging, particularly for tumor regions, where they can be tracked using magnetic resonance imaging (MRI). The unique properties of MNPs, including their ability to be manipulated by external magnetic fields and their relatively small size, make them promising candidates for targeted therapies in oncology. They can potentially deliver diagnostic and therapeutic agents directly to tumor sites, improving the specificity and reducing systemic toxicity.[16] However, a significant challenge remains in the application of metallic nanoparticles in high-grade gliomas, primarily due to the blood-brain tumor barrier (BBTB). Unlike the normal blood-brain barrier (BBB), which limits the penetration of most therapeutic agents into the brain, the BBTB is often more permeable. Yet, this permeability is not uniform across all tumor types, and in high-grade gliomas, the BBTB still presents a major hurdle. The BBTB in gliomas is heterogeneous, with variable vessel structures that can limit the effective accumulation of nanoparticles in tumor tissues. Furthermore, the enhanced permeability and retention (EPR) effect, which is often used to describe the ability of nanoparticles to accumulate more in tumor tissue than in normal tissues, is less effective in high-grade gliomas due to the abnormal vasculature and increased interstitial pressure, which hinder the penetration of nanoparticles into the tumor.[17,18]

In high-grade gliomas, the chaotic nature of the tumor vasculature, along with the presence of glial scar tissue, often restricts the passive diffusion of nanoparticles. The lack of consistent vascular permeability within the tumor means that nanoparticles do not always accumulate effectively in the tumor tissue.[19] Additionally, the increased interstitial fluid pressure within the tumor can act as a barrier, preventing the efficient delivery of nanoparticles through the tumor stroma.[20] Recent literature has addressed these limitations and suggested potential solutions. Some researchers have proposed the use of active targeting strategies, where nanoparticles are functionalized with ligands that specifically recognize receptors overexpressed on tumor cells, allowing for more precise delivery. Additionally, there have been efforts to develop nanoparticles that can overcome the BBTB through external stimuli, such as focused ultrasound or magnetic fields, to temporarily disrupt the BBTB and enhance nanoparticle delivery. These approaches may offer more promising alternatives to passive targeting in the treatment of high-grade gliomas.[21–23]

Magnetic nanoparticles have created new opportunities for cancer diagnosis and therapy, owing to their distinctive physical traits, including their small size, magnetic nature, and biocompatibility.[24] By functionalizing these nanoparticles with targeting ligands, like monoclonal antibodies, their ability to selectively bind to specific molecular and cellular targets in cancer cells can be greatly improved.[16,19,24] Metallic nanoparticles have unique properties, such as ease of functionalization, magnetic responsiveness, and the ability to be monitored through imaging techniques like MRI, making them particularly suitable for both types of targeting.[24–26] However, metallic NPs also face challenges, such as limited penetration into deep tumor tissues and potential toxicity due to their accumulation in non-target organs, which may reduce their therapeutic efficacy.[17,18] Metallic nanoparticles, including gold, silver, and iron nanoparticles, offer significant advantages for both tumor targeting and tumor cell targeting.[26,27] While tumor targeting leverages the EPR effect for passive accumulation in tumor tissues, tumor cell targeting involves active mechanisms, often through functionalization with specific ligands that recognize cancer cell markers.[17,18] By combining these two mechanisms, metallic nanoparticles can be used effectively in cancer therapy, both for general tumor treatment and for more targeted, precise drug delivery to tumor cells uptake. The physicochemical properties of nanoparticles, such as morphology (size, shape), molecular weight, aggregation and agglomeration states, surface charge, chemical purity, and surface modification, influence their cellular uptake, intracellular transport, and cytotoxicity.[28,29] This issue appears to be more complex in the case of MNPs, which are further functionalized on their surface.[30,31] The type of surface functionalization applied, which affects various parameters such as biodistribution, adhesion/penetration of biological membranes, and retention, translates into cytotoxic effects.[30–32] Therefore, determining the potential toxicity of these hybrid nanoparticles has become one of the main challenges especially when targeting to specific surface receptors.

Integrins are a family of transmembrane receptors that possess distinct ligand-binding specificities and function as cell adhesion, migration and signaling in different cancers.[33] Integrins αvβ3 and αvβ5 are particularly involved in survival and apoptosis pathways in glioblastoma cells.[34] In glioblastoma, angiogenesis is notably mediated by integrins αvβ3, αvβ5, αvβ1, and αvβ8, which are involved in tumor-associated blood vessel formation, metastasis, and tumor cell intravasation.[35] The adhesive interactions of integrins αvβ3 and αvβ5 with provisional matrix proteins in the tumor microenvironment provide survival cues and/or traction for invading endothelial cells.[34,36] Integrins β1 and β8 have been also implicated in glioblastoma cell migration and invasion.[37]

In this study, carbon-encapsulated iron nanoparticles functionalized with monoclonal antibodies targeting the beta-3 subunit of the integrin αVβ3 receptor, which is overexpressed in glioblastoma cells, was developed and studied as novel MRI contrast candidates on murine glioma GL261 cells in preclinical models.

Materials and Methods

Materials

The murine glioma cell line (GL261) was obtained as a gift from Dr. Robert Zdanowski (Military Institute of Hygiene and Epidemiology, Warsaw, Poland). Dulbecco's Modified Eagle Medium (DMEM), Phosphate Buffered Saline (PBS), Foetal Bovine Serum (FBS), and antibiotics (streptomycin, 50 $\mu g \cdot mL^{-1}$; amphotericin B, 1.25 $\mu g \cdot mL^{-1}$; gentamicin, 50 $\mu g \cdot mL^{-1}$; penicillin, 50 $U \cdot mL^{-1}$) was purchased from Gibco (Gibco, Paisley, UK). Monoclonal antibodies against the beta-3 subunit (CD61) of the integrin alpha-v-beta-3 were obtained from Beckman Coulter. Sodium phosphate and gelatin type B were purchased from Sigma-Aldrich (Steinheim, Germany). All other reagents were prepared using analytical-grade chemicals. Carbon-encapsulated iron nanoparticles were synthesized and surface-functionalized with monoclonal antibodies against CD61 in our laboratories.[38–44]

Cell Culture and the Internalization Studies

Glioma GL261 cells were plated in 75 mL Tissue Culture Flasks and cultured in DMEM that included 10% FBS, penicillin (100 $U \cdot mL^{-1}$), and streptomycin (100 $\mu g \cdot mL^{-1}$) at 37°C in a 5% CO_2 atmosphere. For the experiments, 0.5×10^5 cells in 500 µL of growth medium were seeded into a single well of a 12-well plate. The culture medium was then removed, and 0.5 mL of a suspension of antibody-functionalized carbon-encapsulated iron nanoparticles (Fe@C-CONH-anti-CD61 or Fe@C-CH_2CH_2CONH-anti-CD61) was added. Non-functionalized carbon-encapsulated

iron nanoparticles (Fe@C) were used as controls. The final nanoparticle concentrations in the wells were 12.5 and 25 μg mL^{-1}. A pure cell control was also included, to which 0.5 mL of PBS was added instead of nanoparticles. After 3 hours of incubation, the medium was collected and centrifuged at 400 g, and the pellet was resuspended in 200 μL of PBS. The adherent cells were treated with trypsin, rinsed twice with PBS, and then resuspended in 200 μL of PBS. The prepared medium, along with pristine Fe@C, Fe@C-CONH-anti-CD61, and Fe@C-$(CH_2)_2$-CONH-anti-CD61 suspensions, was added to gelatin type B to create MRI phantoms.

TEM Analysis

Carbon-encapsulated iron nanoparticles suspended in Milli-Q'water were carefully placed on a carbon pre-coated 300-mesh copper grid for 1 h for visualization by TEM. The research was carried out on a TALOS F200X equipped with a High-Angle Annular Dark-Field detector (FEI, currently Thermo Fisher Scientific). In the cell studies, the GL261 cells were exposed to a suspension of Fe@C-$(CH_2)_2$CONH-MoAb (10 μg mL^{-1}) for 24 hours. After exposure, the GL261 cells were fixed with 2.5% glutaraldehyde cacodylic buffer and incubated for 1 h, then washed in 0.1 M cacodylic buffer. Next the cells were postfixed in 1% OsO_4 in double distilled water (ddH_2O) for 1 h and washed three times in ddH_2O. After post-fixation the samples were dehydrated through a graded series of EtOH (30%–10 min, 50%–10 min, 70%–24 h, 80%–10 min, 90%–10 min, 96%–10 min, anhydrous EtOH – 10 min, acetone – 10 min) and infiltrated with Epon 812 resin in acetone (1:3–30 min, 1:1–30 min, 3:1–2 h), infused twice for 24 h in pure epon resin and polymerized 24 h at 60°C. Next, the 60 nm sections were prepared (RMC ultramicrotome MTX) and examined without contrast under the transmission electron microscope using a JEM-1220 TEM (JEOL).

ICP-MS Analysis

The cells (GL261) were exposed to Fe@C-$(CH_2)_2$CONH-MoAb suspension (10 μg mL^{-1}) for 24 h. After the exposure, the cells were washed twice with cold PBS without Ca/Mg ions and the cell samples were initially digested using an acid solution of concentrated nitric acid (Merck) and mineralized using microwave digestion type UltraWave (Milestone) for 30 min at 210°C. The iron content of incubated GL261 cells was determined using the inductively coupled plasma mass spectrometry (ICP-MS) method (Thermo Electron X Series II, Thermo Electron Corporation, USA). A calibration curve was first established for various known concentrations of iron with indium (Merck) used as internal standard. The concentration of cells was established to ensure that the iron content was within the range of the calibration curve. The samples of mineralized cells (50 mL) were measured in two independent experiments.

MTT Assay

The GL261 cells were exposed to Fe@C-CONH-MoAb and Fe@C-$(CH_2)_2$CONH-MoAb nanoparticles (0.0001–50 μg·mL^{-1}) for 24 hours. After exposure, the medium containing the nanoparticle suspension was removed, and a 0.5 - mg·mL^{-1} MTT solution (Sigma-Aldrich) was added to the cells and incubated for 2 hours. Following incubation, the MTT solution was replaced with acidic isopropanol (0.1 N HCl in absolute isopropanol) to dissolve the resulting formazan crystals. The samples were then centrifuged at 15,000 rpm for 10 minutes. Absorbance values were measured at 570 nm within 1 hour using a microplate reader (BioTek, Synergy 4, Biokom) equipped with Gen5 software (BioTech Instruments, Inc., Biokom), with calibration to zero absorbance using acidic isopropanol. Non-treated glioma cells served as the control. The relative cell viability (%) was calculated as [A]/[B] × 100, where [A] is the absorbance of the test sample and [B] is the absorbance of the control sample containing untreated cells.

LDH Release Assay

The GL261 cells were exposed to Fe@C-CONH-MoAb and Fe@C-$(CH_2)_2$CONH-MoAb nanoparticles (0.0001–50 μg mL^{-1}) for 24 hours. The maximum lactate dehydrogenase (LDH) release was determined after complete cell lysis using Triton X-100 (Sigma-Aldrich). Additionally, cell-free wells containing Fe@C-CONH-MoAb and Fe@C-$(CH_2)_2$CONH-MoAb in the concentration range tested were prepared to account for any absorbance due to the nanoparticles themselves.[43] After exposure, the cell culture medium from each well was carefully removed and centrifuged (4000 rpm for 7 minutes). Aliquots of the supernatant (100 μL) were then transferred to fresh wells of

a 96-well plate and mixed with equal volumes of freshly prepared assay reaction mixture. The microplate was incubated for 30 minutes at room temperature in the dark, as described in the Cytotoxicity Detection Kit LDH protocol (Roche Applied Sciences). Absorbance was measured at 490 nm using a microplate reader (BioTek, Synergy 4, Biokom) equipped with Gen5 software (BioTech Instruments, Inc., Biokom). Nanoparticle-mediated cytotoxicity, expressed as LDH release (%), was calculated using the following equation: [(A test sample – A low control) / (A high control – A low control)] × 100%, where A represents absorbance.

Fluorescent Staining of Live and Dead Cells

Viable and dead cells were observed using a fluorescent microscope with a double-staining method, utilizing the calcein AM/PI kit as per the manufacturer's instructions. After 24 hours of exposure to Fe@C-CONH-MoAb and Fe@C-$(CH_2)_2$CONH-MoAb nanoparticles at concentrations ranging from 0.0001 to 50 $\mu g \cdot mL^{-1}$, the culture medium was removed, and the cells were gently washed with PBS. The cells were then stained with an assay solution containing calcein AM (2 $\mu L \cdot mL^{-1}$) and PI (1 $\mu L \cdot mL^{-1}$) and incubated at 37°C for 15 minutes. Digital images of viable (green fluorescence, excitation: 490 nm, emission: 515 nm) and dead (red fluorescence, excitation: 535 nm, emission: 617 nm) cells in selected areas were captured using phase-contrast inverted microscopy (Nikon Eclipse TS 100 F) equipped with a Nikon Digital Sight DS-U2 camera.

In vitro Relaxometry

Magnetic resonance imaging in vitro was conducted with a 1.5 T (63 MHz) system (Magnetom Avanto, Siemens Medical Solutions, Erlangen, Germany), equipped with explorer gradients (maximum gradients of 40, 40, and 45 mT/m along the x, y, and z axes, respectively, and a slew rate of 200 mT m^{-1} ms^{-1}), and a 32-channel system. A 2-channel volume transceiver coil was used to image gelatin type B phantoms containing GL260 cells. During the MR imaging process, the position of the tube rack inside the tomograph remained fixed and was precisely aligned using a laser system. For T1 measurements, T1-weighted images were obtained using the SE sequence (TR/TE 450/8.4 ms). For T2 measurements, T2-weighted images were captured using a sixteen-echo MRI SE sequence with echo times (TR/TE) of 2000 ms and a range of TE values: 22, 44, 66, 88, 110, 132, 154, 176, 198, 220, 242, 246, 286, 308, 330, 352, 374, 396, 418, 440, 462, 484, 506, 528, 550, 572, 594, 616, 638, 660, 682, and 704 ms. Data acquisition was carried out using the K-PACS Workstation V 1.6.0 software by Image Information System Ltd. The signal intensity for each sample was calculated and used for the mathematical analysis of the relaxation times.

Animals

The investigations were approved by the 2nd Local Ethics Commission at the Medical University of Warsaw, which deals with experiments with laboratory animals (No 3/2009). The preclinical studies were conducted in accordance with the guidelines set by the above Commission, adhering to laws concerning animal welfare and regulations for the care and use of laboratory animals. Female C57BL/6 mice, aged six to eight weeks, were obtained from the Mossakowski Institute of Experimental and Clinical Medicine, Polish Academy of Sciences (Warsaw, Poland). These mice were housed in groups of five in standard cages with *ad libitum* access to food and water and maintained on a 12-hour light/dark cycle. Prior to the experimental procedure, the animals were acclimatized to the facility for at least one week. Mice were randomly assigned to numbered cages and injected subcutaneously in the right flank with 0.5×10^6 GL261 cells suspended in 100 µL sterile PBS. MRI scans were performed on mice with syngeneic tumors four weeks after injection. Prior to each scan, mice were anesthetized with ketamine (45 $mg \cdot kg^{-1}$). The nanomaterial (Fe@C-CH_2CH_2CONH-anti-CD61) was administered intravenously into the tail vain as a single bolus (0.1 mL) at a concentration of 1 $mg \cdot mL^{-1}$ (5 $mg \cdot kg^{-1}$ of mice body weight). Each animal was imaged at baseline (prior to contrast), and then at 15 minutes, 1 hour, 3 hours, 12 hours, and 24 hours following contrast injection. MRI data for each animal were used to generate time curves reflecting changes in T1 and T2 relaxation times for various organs, including the transplanted tumor, spleen, liver, kidney, heart, lung, brain, and soleus muscle. Images from the test animals were compared to the pre-contrast images.

 https://doi.org/10.2147/IJN.S511286

In vivo Relaxometry

In vivo magnetic resonance imaging was conducted using a 1.5 T (63 MHz) system (Magnetom Avanto, Siemens Medical Solutions, Erlangen, Germany). T1-weighted images were acquired using the VIBE sequence (TR/TE 15.00/2.31 ms) at two angles (5° and 26°). T2-weighted imaging was performed with the TSE sequence (TR/TE 3500/63 ms, acquisition time 13:08 minutes, voxel size 0.5×0.5 × 0.1 mm, flip angle 150°, slice thickness 1 mm, with 32 averages). The quantitative analysis of T2 relaxation time (ms) was based on an eight-echo SE sequence (TR 2000 ms, TE values of 22.0, 44.0, 66.0, 88.0, 110.0, 132.0, 154.0, and 176.0 ms), with a total acquisition time of 9:38 minutes, voxel size of 0.8×0.6 × 2.0 mm, flip angle 180°, slice thickness 2 mm, and 4 averages.

Relaxation Times

After acquiring the MR images, the mean signal intensity (INS) was measured within the manually drawn equal-sized regions of interest (ROI) for each tested sample. The relaxation times were calculated by mono-exponential curve fitting of the signal intensity vs time (TI or TE) using the MATLAB software. The following equation was used to fit the curves:

$$S(T_1) = S_0 \times \left|1-2e^{\frac{-T_1}{T_1}} + e^{\frac{-T_R}{T_1}}\right|$$

where S(T1) is the signal intensity with inversion pulse of duration T_1 applied, T_R is the repetition time, S_0 is the proton density, and T_1 is the longitudinal relaxation time. The absolute values account for the fact that the signal intensity in data is represented by the unsigned integer. T_1 was calculated numerically with the nonlinear regression model using the Levenberg-Marquardt algorithm (LMA) to fit the model curve to the experimental data. For the signal intensity function of T2 relaxation, the following equation was used to determine T2 relaxation times:

$$M(T_E) = M_0 e^{\frac{-T_E}{T2}}$$

where TE is the time of echo, T2 is the transversal relaxation time, and M_0 is the proton density.

Statistics

The Shapiro–Wilk test was used to test for normal distribution of data and the Levene's test for homogeneity of variance. Analysis of variance (ANOVA) was used to test for significance between the relaxation times. The nonparametric test of Kruskal–Wallis ANOVA was used when the data did not meet the requirements for the parametric test. Values of $p<0.05$ were considered statistically significant. The analyses were performed using Statistica 13.3 software (StatSoft, Poland).

Results and Discussion

Carbon-encapsulated magnetic nanoparticles decorated with monoclonal antibodies against the beta-3 subunit (CD61) of the integrin alpha-v-beta-3 were investigated as novel contrast agents in murine glioma (GL261). These core-shell type nanoparticles were synthesized by a carbon arc discharge route[38,39] and fully characterized for the size, shape, composition and physicochemical properties as described elsewhere.[40] More details on synthesis setups and purification and characterizations of carbon-encapsulated iron nanoparticles conjugated with and without monoclonal antibodies are also provided in ESI (Figures S1–S16 and Tables S1–S3). Bioconjugation studies on carbon-encapsulated iron nanoparticles have been completed in our previous studies.[41,44] The structures of the designed nanomaterials used in this study are presented in Scheme 1. Notably, to ensure the desired reaction pathway toward the target nanoparticles, at first carboxylic groups on the surface of the nanomaterial was activated using carbodiimide-type reagent to ensure the reaction proceeds with the inclusion of carboxylic groups only on the surface of the nanomaterial with subsequent reaction with amino groups from antibody.

In the present studies, we performed two types of experiments applying murine glioma GL261 cells (in vitro) followed by preclinical (in vivo) using C57BL/6 mice as models. The internalization studies showed that Fe@C-$(CH_2)_2$CONH-MoAb nanoparticles have been loaded as a sediment mass in murine glioma cells. This was evidenced by TEM findings, which show both individual nanoparticles and agglomerates located within the mitochondria and cytoplasm of the glioma cells (Figure 1). Further confirmation of the presence of Fe@C-$(CH_2)_2$CONH-MoAb

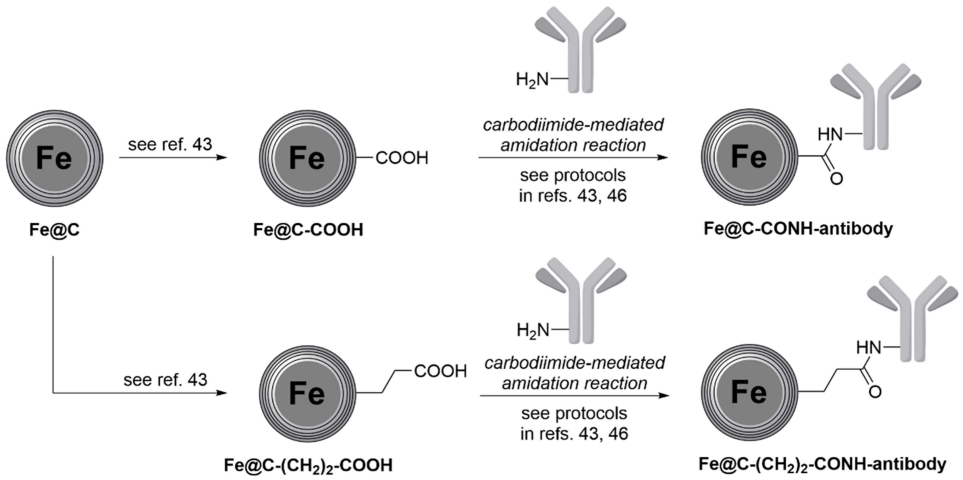

Scheme 1 General synthesis path toward Fe@C-CONH-MoAb and Fe@C-$(CH_2)_2$CONH-MoAb.

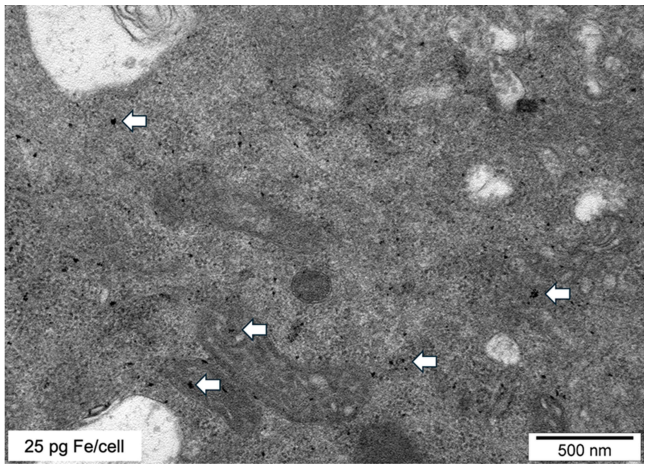

Figure 1 TEM image of murine glioma cells (GL261) after 24h of exposure to Fe@C-$(CH_2)_2$CONH-MoAb nanoparticles (10 μg·mL^{-1}). Arrows show the main direction of nanoparticles internalization within mitochondria and cytoplasm. The Fe content was analyzed by ICP-MS (left insert). Bar is 500 nm. ICP-MS data are mean of three individual samples (n=3).

nanoparticles in the glioma cells was obtained through ICP-MS analysis, which revealed a significant increase of iron in the glioma cells (Figure 1). In control glioma cells treated without nanoparticles, the iron content was approximately 2 pg Fe/cell.[45] After exposure to Fe@C-$(CH_2)_2$CONH-MoAb nanoparticles, the iron content in GL261 cells increased to ca. 25 pg Fe/cell (Figure 1). Based on these quantitative data, we can estimate the average mass loading of Fe@C-$(CH_2)_2$CONH-MoAb nanoparticles that were internalized into the glioma cells in vitro. The iron content measured by ICP-MS indirectly reflects the amount of Fe@C-$(CH_2)_2$CONH-MoAb nanoparticles present inside the cells.

MTT reduction was used to metabolically assess the viability of cancer cells after exposure to Fe@C-CONH-MoAb and Fe@C-$(CH_2)_2$CONH-MoAb. No significant differences in the cytotoxicity profiles were observed in GL261 cells exposed to Fe@C-CONH-MoAb and Fe@C-$(CH_2)_2$CONH-MoAb, although there was a trend suggesting that Fe@C-$(CH_2)_2$CONH-MoAb nanoparticles slightly reduced the cell viability more than Fe@C-CONH-MoAb (Figure 2A). A statistically significant difference was observed only at a concentration of 50 μg·mL^{-1} compared to untreated controls (Figure 2A). Interestingly, our previous cytotoxicity studies on similar carbon-encapsulated iron nanoparticles, non-functionalized with CD61 monoclonal antibodies, showed a significant reduction in MTT at the highest concentrations tested, 50 μg·mL^{-1} and 100 μg· mL^{-1}, in glioma cells.[45] Our findings align with other recent studies on the cytotoxicity of MNPs. Several preclinical studies have

https://doi.org/10.2147/IJN.S511286

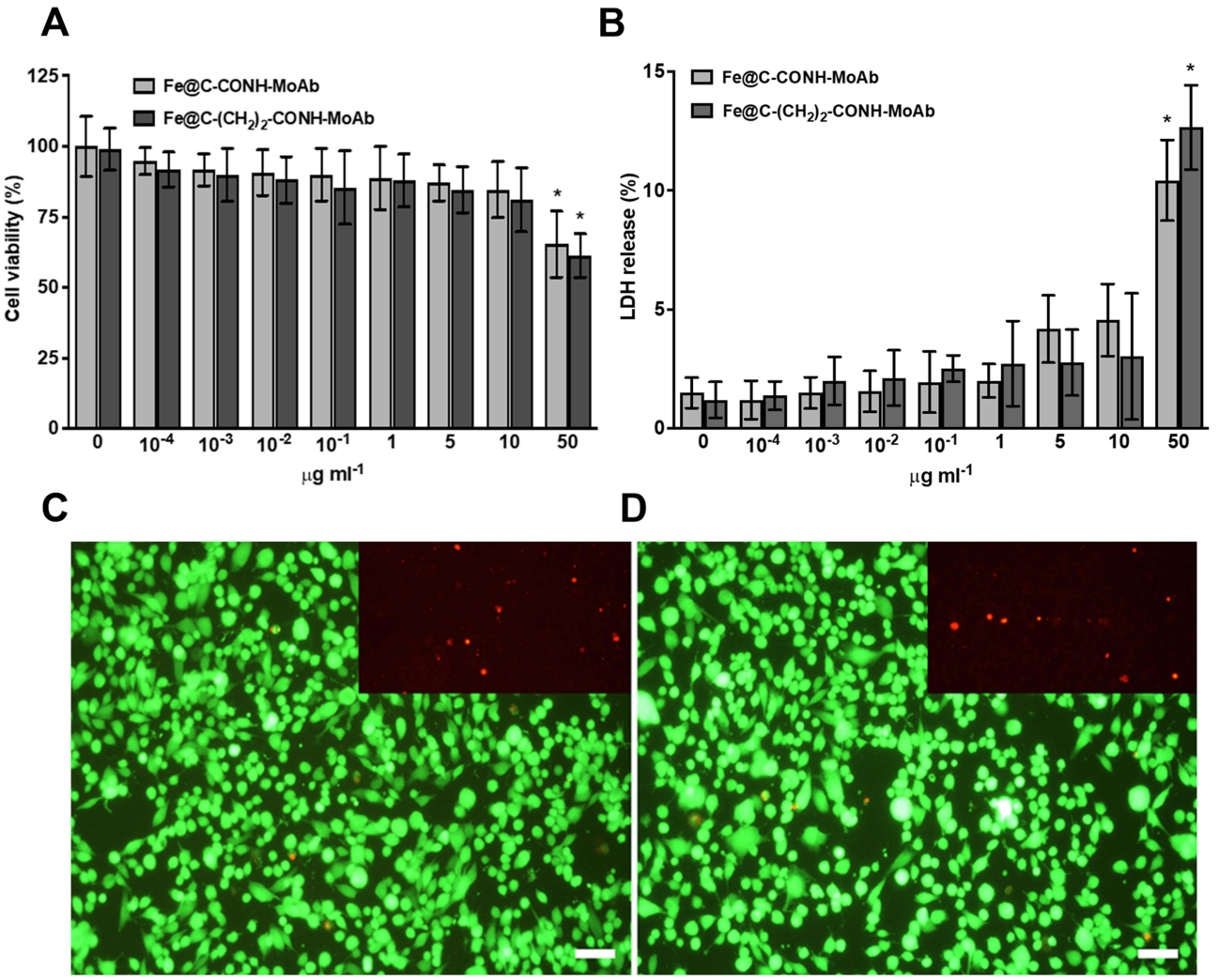

Figure 2 Cellular response of murine glioma cells (GL261) after 24 h of exposure to Fe@C-CONH-MoAb and Fe@C-$(CH_2)_2$CONH-MoAb nanoparticles (0.0001–50 μg·mL^{-1}). (**A**) MTT reduction assay showing cell viability. Results are presented as mean ± SD from three independent experiments, with three replicas per concentration. (*) indicates a statistically significant difference compared to untreated controls ($P < 0.05$). (**B**) LDH leakage assay indicating cell membrane integrity. Results are also expressed as mean ± SD from three independent experiments. (*) denotes statistically significant difference compared to untreated controls ($P < 0.05$). Representative fluorescence images of glioma cells stained with calcein-AM (green) and propidium iodide (red) after exposure to (**C**) Fe@C-CONH-MoAb and (**D**) Fe@C-$(CH_2)_2$CONH-MoAb nanoparticles at 50 μg·mL^{-1}. Inserts show cells stained with propidium iodide (PI). Bar = 50 μm. MTT, 3-(4,5-dimethylthiazol-2-yl)-2,5-diphenyltetrazolium bromide; LDH, lactate dehydrogenase.

shown that iron oxide magnetic nanoparticles, with varying physicochemical properties, exhibited no severe cytotoxicity when used at concentrations below 100 μg·mL^{-1} in glioma and breast cancer cells.[46,47]

Studies have shown that functionalization of MNPs by introducing functional groups of different sizes, such as carboxyl groups, can influence their cytotoxicity.[48,49] Therefore, it was investigated whether the functionalized MNPs used in this experiment would induce cytotoxic effects by disrupting the plasma membrane in GL261 cells. To elucidate membrane-targeted cytotoxic endpoints, we applied colorimetric LDH leakage and Calcein-AM/PI fluorescence staining methods. The LDH assay revealed significant cytotoxicity of the tested nanomaterials only at the highest concentration of 50 μg mL^{-1} (Figure 2B), which was consistent with the cell viability profile obtained from the MTT assay (Figure 2A). These results were further confirmed by our double-staining protocols using calcein-AM and propidium iodide. When the cells were treated with both Fe@C-CONH-MoAb and Fe@C-$(CH_2)_2$CONH-MoAb at 50 μg mL^{-1}, a significant decrease in membrane integrity was observed in glioma cells (Figure 2C). This was also accompanied by an increase in propidium iodide-stained cells (Figure 2D).

The relaxation study was performed using pristine nanoparticles (Fe@C) and functionalized nanoparticles with monoclonal antibodies (CD61) attached to the carbon surface through the short (Fe@C-CONH-anti-CD61) and long (Fe@C-$(CH_2)_2$-CONH-anti-CD61) aliphatic linkers. Representative T2-weighted images of glioma cells treated with and without nanoparticles coupled to antibodies are shown in Figure 3A and B. It was found that nanoparticles decorated with antibodies diminished relaxation signals resulting as a dark spot on T2-weighted images. This effect was not observed on T1-weighted images confirming a typical negative contrast enhancing effects (Figures S17 and S18). Note that the T2 contrast enhancement effect of the tested nanoparticles is directly dependent on iron concentration, which is found in agreement with other recent studies.[50–52]

Recent studies have demonstrated that nanoparticles functionalized with antibodies can significantly reduce relaxation signals, resulting in dark spots on T2-weighted MRI images. This effect is typical of negative contrast agents. However, this phenomenon was not observed in T1-weighted images, which confirms the typical behavior of nanoparticles as negative contrast agents in T2-weighted imaging.[53] It is important to note, however, that smaller nanoparticles, particularly those with high magnetic moments, can exhibit positive contrast on T1-weighted images.[54] These nanoparticles can shorten the T1 relaxation time of surrounding water protons, leading to an increase in signal intensity resulting in a brighter appearance, or positive contrast, on the T1-weighted images. This positive contrast effect can be particularly pronounced in smaller nanoparticles due to their higher surface area-to-volume ratio and enhanced interaction with the magnetic field, which may result in a greater reduction in T1 relaxation time. The size and surface characteristics of the nanoparticles play a critical role in determining whether they will predominantly enhance T1 or T2 contrast. Therefore, while large nanoparticles tend to show negative contrast on T2-weighted images, smaller nanoparticles can provide positive contrast on T1-weighted images due to their distinct magnetic properties.[55] Smaller nanoparticles, particularly those designed to have a high magnetic moment (such as superparamagnetic iron oxide nanoparticles), can display different contrast enhancement behavior on T1-weighted images compared to larger nanoparticles, which might not show such pronounced positive contrast. This distinction should be carefully considered when selecting nanoparticles for specific MRI applications, particularly in diagnostic imaging.[56]

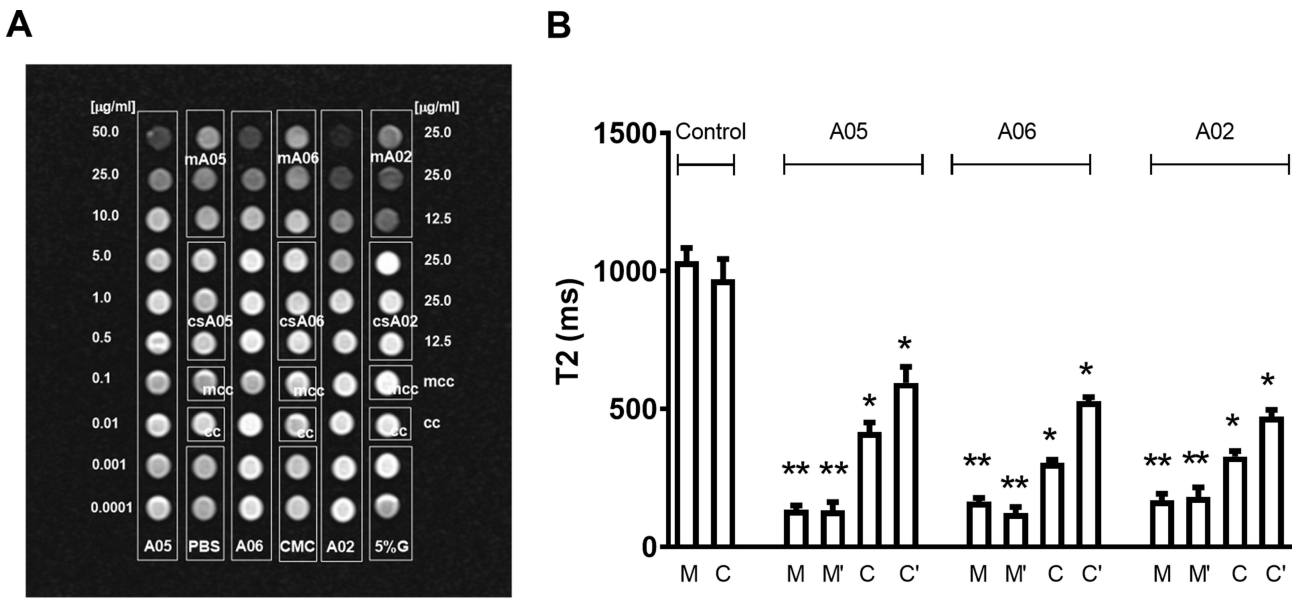

Figure 3 (**A**) T2-weighted images of the gelatin phantoms for Fe@C (A02), Fe@C-CONH-anti-CD61 (A05) and Fe@C-$(CH_2)_2$-CONH-anti-CD61 (A06) nanoparticles and collected medium samples MRI phantom studies in GL261 glioma cells and m – medium, cs – GL261 cells, mcc – medium collected from control cells, cc - control cells, not exposed to Fe@C-CONH-anti-CD61, (**B**) T2 relaxation times values of GL261 cells and collected medium samples after 3hs incubation with Fe@C-CONH-anti-CD61 (A05) and Fe@C-$(CH_2)_2$-CONH-anti-CD61 (A06) nanoparticles. C- cells and M-, medium after incubation with Fe@C-CONH-anti-CD61 in concentration 25 µg·mL-1, C' -cells, M'-medium after incubation with Fe@C-CONH-anti-CD61 in concentration 12.5 µg·mL^{-1}. Results represent mean ± SD (n=10). (*) P<0.05 within group, (**) P<0.05 versus control group.

https://doi.org/10.2147/IJN.S511286

The performed phantom studies showed the selective imaging of glioma on T2-weighted images using nanoparticles coupled with monoclonal antibodies. One has to be noted that darkening of the image is observed not only for the imaged cells, but also within the tested medium collected after incubation with cells, which indicates incomplete binding of anti-CD61 functionalized contrasts to the integrin on the surface of GL261 cells (Figure 3). The performed studies evidence that nanoparticles functionalized with monoclonal antibodies against the beta-3 subunit of αVβ3 integrin reduce the T2 relaxation times on T2-weighted images (Figure 3). The reduced values of T2 relaxation times were also obtained for the medium collected after incubation of cells with nanomaterials, which is consistent with data on qualitative phantom images (Figure 3A and B). No such effects were demonstrated on T1 relaxation times (Figures S17 and S18).

Preclinical MRI studies were performed on C57BL/6 mice bearing GL261 glioma on right flank and imaged without and with nanoparticles (Fe@C-$(CH_2)_2$-CONH-anti-CD61) dosed intravenously in a single bolus to tail vain at dose of 5 $mg \cdot kg^{-1}$ of mice body weight. Post-contrast T1- and T2-weighted images were acquired on mice and T1 and T2 relaxation times were calculated for tumor tissues and body organs such as liver, spleen, kidney, heart, lung, brain and soleus muscle. Studies evidence that nanoparticles led to a reduction of T2 relaxation time in glioblastoma over the entire range of the analysed time interval (Figure 4A). The highest decrease in the value of T2 relaxation time was recorded at 12 and 24 hours after the administration of nanoparticles. Except for the intermittent decrease in T2 time at 12 hours in the liver (Figure 4B), no decrease in T2 relaxation time was observed in other organs (data not shown). There were also no changes in the T1 relaxation time after the administration of nanoparticles in the studied glioblastoma tumors and in all the examined organs in mice bearing glioblastoma. The designed Fe@C-$(CH_2)_2$-CONH-anti-CD61 conjugates demonstrated high efficiency as a negative contrast agent possessing relaxometry effects comparable to surface engineered iron oxide nanoparticles.[57,58] This is confirmed by T2-images of mice with pre- and post-nanoparticle dosages (Figure 4C and D).

In this study, we utilized magnetic nanoparticles (MNPs) functionalized with CD61 to target the αvβ3 integrin for enhanced MRI diagnostics in GL261 tumor models. The choice of CD61 as a targeting ligand was based on its ability to bind to integrin αvβ3, which is overexpressed in gliomas and other types of tumors. Integrin αvβ3 plays a crucial role in tumor cell adhesion, migration, and angiogenesis, making it an attractive target for cancer diagnostics and therapy.[33,36,59,60] By functionalizing MNPs with CD61, we aimed to selectively bind these nanoparticles to tumor cells expressing αvβ3 integrin, thereby improving the specificity and sensitivity of MRI imaging in the detection of glioma and other cancer types.[12,16,61] While the tumors in our study were located in the flank, rather than in the brain, we emphasize that the blood-brain barrier (BBB) was not relevant for this particular model. In contrast to brain tumors, flank-located tumors do not require overcoming the BBB for nanoparticle delivery. However, the delivery of nanoparticles to flank tumors is influenced by other factors such as tumor vasculature, interstitial pressure and first-pass liver effects. The Enhanced Permeability and Retention (EPR) effect allows nanoparticles to accumulate in tumor tissue due to the abnormal and leaky blood vessels characteristic of tumors.[17,18] Despite this, the interstitial pressure within tumors can limit the penetration of nanoparticles, which is a common challenge in nanoparticle-based therapies and diagnostics.[17,20]

In terms of diagnostic applications, magnetic nanoparticles have the advantage of being detectable by MRI, which allows for non-invasive monitoring of tumor growth and response to treatment. The magnetic properties of these nanoparticles enhance the contrast in MRI images, facilitating improved tumor visualization and detection.[25,62,63] Although our study did not involve external magnetic field guidance, the inherent magnetic properties of the nanoparticles still provide significant value for diagnostic imaging, particularly in the context of targeted tumor imaging. Note that the reticuloendothelial system (RES) plays an important role in the systemic clearance of nanoparticles, and non-specific uptake by the RES can limit the effective concentration of nanoparticles at the tumor site.[24,61,64] However, by functionalizing the nanoparticles with CD61, we improved the targeting specificity of the nanoparticles to αvβ3 integrin-expressing tumor cells, which helps to reduce off-target effects and enhance the diagnostic efficiency of MRI in tumor imaging.[65,66]

In conclusion, our study highlights the potential of CD61-functionalized carbon-encapsulated iron nanoparticles for targeted MRI diagnostics, particularly for gliomas and plausibly other tumors overexpressing the αvβ3 integrin transmembrane receptors. This work underscores the importance of nanoparticle functionalization in improving diagnostic accuracy and providing a non-invasive tool for cancer detection and monitoring.

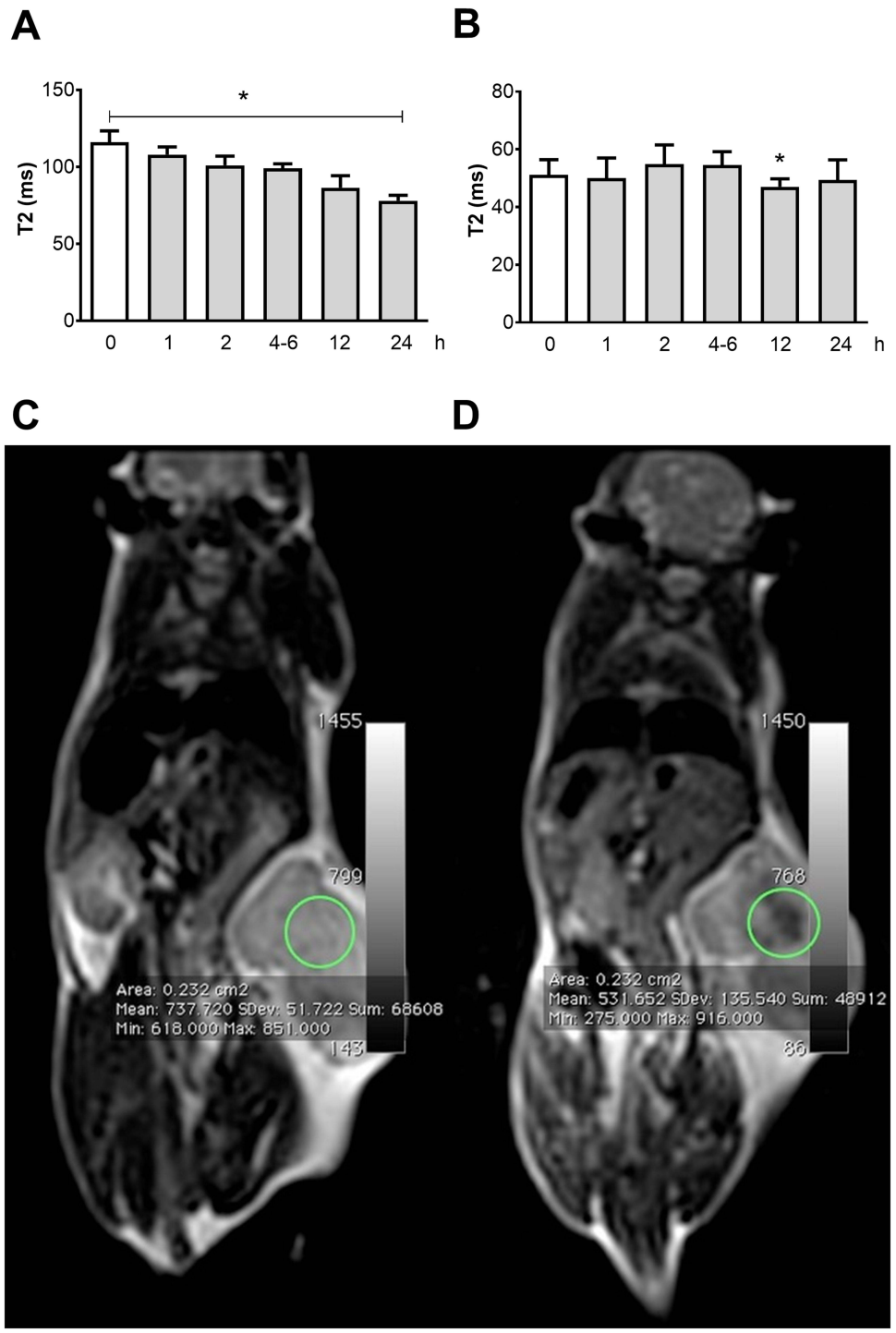

Figure 4 T2 relaxation times of syngeneic glioma (**A**) and liver (**B**) in C57BL/6 mice after intravenous administration of Fe@C-$(CH_2)_2$-CONH-anti-CD61 (A06) nanoparticles as a single bolus (0.1 mL) into the tail vain (1 mg·mL^{-1}, 5 mg kg^{-1} b.w.). (**C**) and (**D**) Representative T2-weighted images of murine glioma (GL261) before (left panel) and after (right panel) nanoparticle administration. The right image shows significant post-contrast darkening in the tumor area (please see ROI - Region of Interest marked as green circle; signal intensity is calculated for selected ROI area 0.232 cm^{-2}), taken 24 hours after intravenous administration of Fe@C-$(CH_2)_2$-CONH-anti-CD61 nanoparticles as a single bolus (0.1 mL) into the tail vain (1 mg·mL^{-1}, 5 mg kg^{-1} b.w.). The left image was taken before nanoparticle administration. T2 relaxation times were quantitatively analyzed based on T2-dependent in eight echo SE sequence images (TR 2000 ms, TE 22.0, 44.0, 66.0, 88.0, 110.0, 132.0, 154.0, 176.0 ms, TA 9:38 min, voxel size 0.8×0.6x2.0 mm, flip angle 180°, slice thickness 2 mm, averages 4). The results represent mean values ± SD (n=6). Statistical significance (* $p<0.05$) is indicated relative to pre-administration groups. MRI was performed on a 1.5 T MR scanner (AVANTO SQ-Engine TIM, SIEMENS, Erlangen, Germany) using TSE sequences (TR/TE 3500/63 ms, voxel size 0.5×0.5x1.0 mm, flip angle 150°, slice thickness 1.0 mm, averages 32).

https://doi.org/10.2147/IJN.S511286

Conclusion

Carbon-encapsulated iron nanoparticles developed in this study showed promise in murine glioma tracking based on specific direct targeting with monoclonal antibodies recognizing integrin alpha-v-beta-3 receptors containing the beta-3 subunit. The as-synthesized nanoparticles were successfully functionalized with monoclonal antibodies, and their resonance properties were tested using a 1.5 T (63 MHz) MRI scanner.

Our findings support the promising potential of magnetic nanoparticles functionalized with CD61 for targeted imaging of gliomas. By targeting the overexpressed αvβ3 integrin, these nanoparticles can improve the specificity and sensitivity of MRI diagnostics, enabling earlier and more accurate detection of integrin receptors in gliomas. This approach also demonstrates how nanoparticle functionalization can overcome the challenges of non-specific accumulation and improve the targeting of tumor sites expressing integrins. Moreover, studies showed that antibody-decorated nanoparticles did not produce any severe cytotoxic effects on murine glioma cells, although some pronounced cytotoxicity was observed with higher applied dose (50 μg mL^{-1}). The non-invasive nature of MRI-based diagnostics, coupled with the ability to specifically target cancer cells, makes this method a valuable tool for personalized cancer diagnostics and monitoring. Future work will focus on further optimizing nanoparticle delivery systems to enhance tumor-specific accumulation and reduce systemic toxicity, ultimately improving the clinical applicability of this technology in modern oncology.

Acknowledgments

The authors thank Dr. Maciej Gawlak for confocal microscopy analysis.

Funding

This study was supported by the National Science Center Grant N N518 381737.

Disclosure

The authors declare that there are no conflicts of interest.

References

1. Incekara F, Koene S, Ajpe V, van den Bent MJ, Smits M. Association between supratotal glioblastoma resection and patient survival: a systematic review and meta-analysis. *World Neurosurg*. 2019;127:617. doi:10.1016/j.wneu.2019.04.092
2. Lin S, Xu H, Zhang A, et al. Prognosis analysis and validation of m(6)A signature and tumor immune microenvironment in glioma. *Front Oncol*. 2020;10:541401. doi:10.3389/fonc.2020.541401
3. Thenuwara G, Curtin J, Tian F. Advances in diagnostic tools and therapeutic approaches for gliomas: a comprehensive review. *Sensors*. 2023;23 (24):9842. doi:10.3390/s23249842
4. Wang LM, Englander ZK, Miller ML, Bruce JN. Malignant Glioma. *Adv Exp Med Biol*. 2023;1405:1–30. doi:10.1007/978-3-031-23705-8_1
5. Yang Y, He MZ, Li T, Yang X. MRI combined with PET-CT of different tracers to improve the accuracy of glioma diagnosis: a systematic review and meta-analysis. *Neurosurg Rev*. 2019;42(2):185–195. doi:10.1007/s10143-017-0906-0
6. Perkins A, Liu G. Primary brain tumors in adults: diagnosis and treatment. *Am Fam Physician*. 2016;93(3):211–217.
7. de Haan J, Vandecaveye V, Han SN, Van de Vijver KK, Amant F. Difficulties with diagnosis of malignancies in pregnancy. *Best Pract Res Clin Obstet Gynaecol*. 2016;33:19–32. doi:10.1016/j.bpobgyn.2015.10.005
8. Li G, Li L, Li Y, et al. An MRI radiomics approach to predict survival and tumour-infiltrating macrophages in gliomas. *Brain*. 2022;145 (3):1151–1161. doi:10.1093/brain/awab340
9. Suh JH, Kotecha R, Chao ST, Ahluwalia MS, Sahgal A, Chang EL. Current approaches to the management of brain metastases. *Nat Rev Clin Oncol*. 2020;17(5):279–299. doi:10.1038/s41571-019-0320-3
10. Upadhyay N, Waldman AD. Conventional MRI evaluation of gliomas. *Br J Radiol*. 2011;84(Spec Iss 2):S107–11. doi:10.1259/bjr/65711810
11. d'Angelo M, Castelli V, Benedetti E, et al. Theranostic nanomedicine for malignant gliomas. *Front Bioeng Biotechnol*. 2019;7:325. doi:10.3389/fbioe.2019.00325
12. El Kheir W, Marcos B, Virgilio N, Paquette B, Faucheux N, Lauzon MA. Drug delivery systems in the development of novel strategies for glioblastoma treatment. *Pharmaceutics*. 2022;14(6). doi:10.3390/pharmaceutics14061189
13. Alabousi M, Davenport MS. Use of intravenous gadolinium-based contrast media in patients with kidney disease and the risk of nephrogenic systemic fibrosis: radiology in training. *Radiology*. 2021;300(2):279–284. doi:10.1148/radiol.2021210044
14. Bhojani MS, Van Dort M, Rehemtulla A, Ross BD. Targeted imaging and therapy of brain cancer using theranostic nanoparticles. *Mol Pharm*. 2010;7(6):1921–1929. doi:10.1021/mp100298r
15. Mattei TA, Rehman AA. "Extremely minimally invasive": recent advances in nanotechnology research and future applications in neurosurgery. *Neurosurg Rev*. 2015;38(1):27–37. doi:10.1007/s10143-014-0566-2

16. Lei J, Huang YY, Zhao YC, Zhou Z, Mao L, Liu YH. Nanotechnology as a new strategy for the diagnosis and treatment of gliomas. *J Cancer*. 2024;15(14):4643–4655. doi:10.7150/jca.96859
17. Bertrand N, Wu J, Xu X, Kamaly N, Farokhzad OC. Cancer nanotechnology: the impact of passive and active targeting in the era of modern cancer biology. *Adv Drug Deliv Rev*. 2014;66:2–25. doi:10.1016/j.addr.2013.11.009
18. Shi Y, van der Meel R, Chen X, Lammers T. The EPR effect and beyond: strategies to improve tumor targeting and cancer nanomedicine treatment efficacy. *Theranostics*. 2020;10(17):7921–7924. doi:10.7150/thno.49577
19. ter Linden E, Abels ER, van Solinge TS, Neefjes J, Broekman MLD. Overcoming barriers in glioblastoma-advances in drug delivery strategies. *Cells*. 2024;13(12):998. doi:10.3390/cells13120998
20. Duan MY, Cao RN, Yang Y, et al. Blood-brain barrier conquest in glioblastoma nanomedicine: strategies, clinical advances, and emerging challenges. *Cancers*. 2024;16(19):3300. doi:10.3390/cancers16193300
21. Rivera-Caraballo KA, Nair M, Lee TJ, Kaur B, Yoo JY. The complex relationship between integrins and oncolytic herpes simplex virus 1 in high-grade glioma therapeutics. *Molecular Therapy-Oncolytics*. 2022;26:63–75. doi:10.1016/j.omto.2022.05.013
22. Sagberg LM, Iversen DH, Fyllingen EH, Jakola AS, Reinertsen I, Solheim O. Brain atlas for assessing the impact of tumor location on perioperative quality of life in patients with high-grade glioma: a prospective population-based cohort study. *Neuroimage-Clinical*. 2019;2019:21101658. doi:10.1016/j.nicl.2019.101658
23. Wang YH, Zhang FC, Xiong NX, et al. Remodelling and treatment of the blood-brain barrier in glioma. *Cancer Manage Res*. 2021;13:4217–4232. doi:10.2147/cmar.S288720
24. Rezaei B, Yari P, Sanders SM, et al. Magnetic nanoparticles: a review on synthesis, characterization, functionalization, and biomedical applications. *Small*. 2024;20(5):e2304848. doi:10.1002/smll.202304848
25. Ramazanov M, Karimova A, Shirinova H. Magnetism for Drug Delivery, MRI and Hyperthermia Applications: a Review. *Biointerf Res Appl Chem*. 2021;11(2):8654–8668. doi:10.33263/briac112.86548668
26. Akhtar N, Mohammed HA, Yusuf M, Al-Subaiyel A, Sulaiman GM, Khan RA. SPIONs conjugate supported anticancer drug doxorubicin's delivery: current status, challenges, and prospects. *Nanomaterials*. 2022;12(20):3686. doi:10.3390/nano12203686
27. Khizar S, Ahmad NM, Zine N, Jaffrezic-Renault N, Errachid-el-salhi A, Elaissari A. Magnetic nanoparticles: from synthesis to theranostic applications. *ACS Appl Nano Mater*. 2021;4(5):4284–4306. doi:10.1021/acsanm.1c00852
28. Raja G, Jang YK, Suh JS, Kim HS, Ahn SH, Kim TJ. Microcellular environmental regulation of silver nanoparticles in cancer therapy: a critical review. *Cancers*. 2020;12(3):664. doi:10.3390/cancers12030664
29. Nel AE, Mädler L, Velegol D, et al. Understanding biophysicochemical interactions at the nano-bio interface. *Nat Mater*. 2009;8(7):543–557. doi:10.1038/nmat2442
30. Panariti A, Miserocchi G, Rivolta I. The effect of nanoparticle uptake on cellular behavior: disrupting or enabling functions? *Nanotechnol Sci Appl*. 2012;5:87–100. doi:10.2147/nsa.S25515
31. Barrera G, Serpe L, Celegato F, et al. Surface modification and cellular uptake evaluation of Au-coated Ni(80)Fe(20) nanodiscs for biomedical applications. *Interface Focus*. 2016;6(6):20160052. doi:10.1098/rsfs.2016.0052
32. Mohammad Awashra PM, Młynarz P. The toxicity of nanoparticles and their interaction with cells: an in vitro metabolomic perspective. *Nanoscale Adv*. 2023;5(10):2674–2723. doi:10.1039/D2NA00534D
33. Liu FF, Wu Q, Dong ZG, Liu KD. Integrins in cancer: emerging mechanisms and therapeutic opportunities. *Pharmacol Ther*. 2023;247108458. doi:10.1016/j.pharmthera.2023.108458
34. Desgrosellier JS, Cheresh DA. Integrins in cancer: biological implications and therapeutic opportunities. *Nat Rev Cancer*. 2010;10(1):9–22. doi:10.1038/nrc2748
35. Li YC, Xie MM, Jones JB, et al. Targeted delivery of DNA topoisomerase inhibitor SN38 to intracranial tumors of glioblastoma using sub-5 ultrafine iron oxide nanoparticles. *Adv Healthcare Mater*. 2022;11(14):2102816. doi:10.1002/adhm.202102816
36. Paolillo M, Serra M, Schinelli S. Integrins in glioblastoma: still an attractive target? *Pharmacol Res*. 2016;113(Pt A):55–61. doi:10.1016/j.phrs.2016.08.004
37. Malric L, Monferran S, Gilhodes J, et al. Interest of integrins targeting in glioblastoma according to tumor heterogeneity and cancer stem cell paradigm: an update. *Oncotarget*. 2017;8(49):86947–86968. doi:10.18632/oncotarget.20372
38. Borysiuk J, Grabias A, Szczytko J, Bystrzejewski M, Twardowski A, Lange H. Structure and magnetic properties of carbon encapsulated Fe nanoparticles obtained by arc plasma and combustion synthesis. *Carbon*. 2008;46(13):1693–1701. doi:10.1016/j.carbon.2008.07.011
39. Bystrzejewski M, Huczko A, Lange H. Arc plasma route to carbon-encapsulated magnetic nanoparticles for biomedical applications. *Sens Actuat B-Chem*. 2005;109(1):81–85. doi:10.1016/j.snb.2005.03.029
40. Grudzinski IP, Bystrzejewski M, Bogorodzki P, et al. Comprehensive magnetic resonance characteristics of carbon-encapsulated iron nanoparticles: a new frontier for the core-shell-type contrast agents. *J Nanopart Res*. 2020;22(4):82. doi:10.1007/s11051-020-04795-w
41. Kasprzak A, Poplawska M, Bystrzejewski M, Grudzinski IP. Sulfhydrylated graphene-encapsulated iron nanoparticles directly aminated with polyethylenimine: a novel magnetic nanoplatform for bioconjugation of gamma globulins and polyclonal antibodies. *J Mat Chem B*. 2016;4(33):5593–5607. doi:10.1039/c6tb00838k
42. Kasprzak A, Poplawska M, Bystrzejewski M, Labedz O, Grudzinski IP. Conjugation of polyethylenimine and its derivatives to carbon-encapsulated iron nanoparticles. *RSC Adv*. 2015;5(104):85556–85567. doi:10.1039/c5ra17912b
43. Han X, Gelein R, Corson N, et al. Validation of an LDH assay for assessing nanoparticle toxicity. *Toxicology*. 2011;287(1–3):99–104. doi:10.1016/j.tox.2011.06.011
44. Poplawska M, Bystrzejewski M, Grudzinski IP, Cywinska MA, Ostapko J, Cieszanowski A. Immobilization of gamma globulins and polyclonal antibodies of class IgG onto carbon-encapsulated iron nanoparticles functionalized with various surface linkers. *Carbon*. 2014;74:180–194. doi:10.1016/j.carbon.2014.03.022
45. Grudzinski IP, Bystrzejewski M, Cywinska MA, et al. Comparative cytotoxicity studies of carbon-encapsulated iron nanoparticles in murine glioma cells. *Colloids Surf B Biointerfaces*. 2014;117:135–143. doi:10.1016/j.colsurfb.2014.02.015
46. Ankamwar B, Lai TC, Huang JH, et al. Biocompatibility of Fe(3)O(4) nanoparticles evaluated by in vitro cytotoxicity assays using normal, glia and breast cancer cells. *Nanotechnology*. 2010;21(7):75102. doi:10.1088/0957-4484/21/7/075102

47. Karlsson HL, Cronholm P, Gustafsson J, Möller L. Copper oxide nanoparticles are highly toxic: a comparison between metal oxide nanoparticles and carbon nanotubes. *Chem Res Toxicol*. 2008;21(9):1726–1732. doi:10.1021/tx800064j
48. Hong SC, Lee JH, Lee J, et al. Subtle cytotoxicity and genotoxicity differences in superparamagnetic iron oxide nanoparticles coated with various functional groups. *Int J Nanomed*. 2011;6:3219–3231. doi:10.2147/ijn.S26355
49. Singh SK, Singh MK, Nayak MK, et al. Thrombus inducing property of atomically thin graphene oxide sheets. *ACS Nano*. 2011;5(6):4987–4996. doi:10.1021/nn201092p
50. Chen L, Xie J, Wu HA, et al. Improving sensitivity of magnetic resonance imaging by using a dual-targeted magnetic iron oxide nanoprobe. *Colloids Surf B Biointerfaces*. 2018;161:339–346. doi:10.1016/j.colsurfb.2017.10.059
51. Minaei SE, Khoei S, Khoee S, Mahdavi SR. Sensitization of glioblastoma cancer cells to radiotherapy and magnetic hyperthermia by targeted temozolomide-loaded magnetite tri-block copolymer nanoparticles as a nanotheranostic agent. *Life Sci*. 2022;306120729. doi:10.1016/j.lfs.2022.120729
52. Kharey P, Goel M, Husain Z, et al. Green synthesis of biocompatible superparamagnetic iron oxide-gold composite nanoparticles for magnetic resonance imaging, hyperthermia and photothermal therapeutic applications. *Mater Chem Phys*. 2023:293126859. doi:10.1016/j.matchemphys.2022.126859.
53. Geraldes C. Rational design of magnetic nanoparticles as T_1-T_2 dual-mode MRI contrast agents. *Molecules*. 2024;29(6):1352. doi:10.3390/molecules29061352
54. Oberdick SD, Jordanova KV, Lundstrom JT, et al. Iron oxide nanoparticles as positive T_1 contrast agents for low-field magnetic resonance imaging at 64 mT. *Sci Rep*. 2023;13(1):11520. doi:10.1038/s41598-023-38222-6
55. Mahbuba R. Magnetic resonance imaging and iron-oxide nanoparticles in the era of personalized medicine. *Nanotheranostics*. 2023;7(4):424. doi:10.7150/ntno.86467
56. Issa B, Obaidat IM, Albiss BA, Haik Y. Magnetic nanoparticles: surface effects and properties related to biomedicine applications. *Int J mol Sci*. 2013;14(11):21266–21305. doi:10.3390/ijms141121266
57. Kaliamurthi S, Demir-Korkmaz A, Selvaraj G, et al. Viewing the emphasis on state-of-the-art magnetic nanoparticles: synthesis, physical properties, and applications in cancer theranostics. *Curr Pharm Des*. 2019;25(13):1505–1523. doi:10.2174/1381612825666190523105004
58. Shevtsov M, Multhoff G. Recent developments of magnetic nanoparticles for theranostics of brain tumor. *Current Drug Metabolism*. 2016;17(8):737–744. doi:10.2174/1389200217666160607232540
59. Bello L, Francolini M, Marthyn P, et al. alpha v beta 3 and alpha v beta 5 integrin expression in glioma periphery. *Neurosurgery*. 2001;49(2):380–389. doi:10.1097/00006123-200108000-00022
60. D'Abaco GM, Kaye AH. Integrins: molecular determinants of glioma invasion. *J Clin Neurosci*. 2007;14(11):1041–1048. doi:10.1016/j.jocn.2007.06.019
61. Xie LQ, Jin WW, Chen HL, Zhang QQ. Superparamagnetic iron oxide nanoparticles for cancer diagnosis and therapy. *J Biomed Nanotechnol*. 2019;15(2):215–235. doi:10.1166/jbn.2019.2678
62. Gao ZY, Ma TC, Zhao EY, et al. Small is smarter: nano MRI contrast agents - advantages and recent achievements. *Small*. 2016;12(5):556–576. doi:10.1002/smll.201502309
63. Wang YXJ. Superparamagnetic iron oxide based MRI contrast agents: current status of clinical application. *Quan Imag Med Surg*. 2011;1(1):35–40. doi:10.3978/j.issn.2223-4292.2011.08.03
64. Wang JTW, Cabana L, Bourgognon M, et al. Magnetically decorated multiwalled carbon nanotubes as dual MRI and SPECT contrast agents. *Advanced Functional Materials*. 2014;24(13):1880–1894. doi:10.1002/adfm.201302892
65. Alday-Parejo B, Stupp R, Ruegg C. are integrins still practicable targets for anti-cancer therapy? *Cancers*. 2019;11(7):978. doi:10.3390/cancers11070978
66. Zhang F, Huang XL, Zhu L, et al. Noninvasive monitoring of orthotopic glioblastoma therapy response using RGD-conjugated iron oxide nanoparticles. *Biomaterials*. 2012;33(21):5414–5422. doi:10.1016/j.biomaterials.2012.04.032